ELSEVIER

Computational Materials Science 27 (2003) 351–374

COMPUTATIONAL MATERIALS SCIENCE

www.elsevier.com/locate/commatsci

Some elements of microstructural mechanics

G. Cailletaud [a], S. Forest [a,*], D. Jeulin [b], F. Feyel [a,c], I. Galliet [a], V. Mounoury [a], S. Quilici [a]

[a] *Centre des Matériaux, Ecole des Mines de Paris/CNRS, UMR 7633, BP 87, F-91003 Evry, France*
[b] *Centre de Morphologie Mathématique, Ecole des Mines de Paris, 35 rue Saint-Honoré, F-77305 Fontainebleau, France*
[c] *ONERA DMSE/LCME, 22 Avenue de la Division Leclerc, BP 72, F-92322 Châtillon Cedex, France*

Received 15 April 2002; received in revised form 14 October 2002; accepted 10 November 2002

Abstract

Microstructural mechanics combines the computational methods of structural mechanics and materials sciences. It is dedicated to the mechanics of heterogeneous materials. On the one hand, it can be used to compute industrial components for which the size of the heterogenities is of the order of magnitude of the size of the structure itself or of holes or notches. On the other hand, the computation of representative volume elements of heterogeneous materials enables one to predict the influence of phase morphology and distribution on the linear or non-linear effective properties, having in view microstructure optimization. Such computations provide the local stress–strain fields that can be used to predict damage or crack initiation. This work focuses on the modern tools available for reconstructing realistic three-dimensional microstructures and for computing them, including parallel computing. The choice of the local non-linear constitutive equations and the difficulty of identification of the corresponding parameters remain the weakest link in the methodology. The main example detailed in this work deals with polycrystalline plasticity and illustrates the tremendous heterogeneity of local stress and strain, and the effect of grain boundary or free surfaces. The computations are finally used to calibrate a simplified homogenization polycrystal model.

Keywords: Structural mechanics; Microstructures; Materials; Parallel computing; Finite element; Constitutive behaviour; Viscoplasticity; Polycrystal

1. Objectives

The mechanics of heterogeneous materials has longly been limited to the derivation of simplified schemes to include some aspects of the microstructure into the prediction of their effective properties [1]. The tremendous increase of computational capabilities has strongly favoured the development of numerical simulations based on a more realistic description of microstructure. The computation of microstructures within the framework of continuum mechanics has now gained the level of a scientific "discipline" in its own. We call it in this work "microstructural mechanics", as a reference to the longstanding and now classical structural mechanics. Microstructural mechanics combines the tools of computational structural

* Corresponding author. Tel.: +33-1-6076-3051; fax: +33-1-6076-3150.
E-mail address: samuel.forest@mat.ensmp.fr (S. Forest).

0927-0256/03/$ - see front matter
doi:10.1016/S0927-0256(03)00041-7

mechanics and materials sciences in order to reach the following objectives:

- *The understanding of local deformation mechanisms* at work in heterogeneous materials at the level of individual heterogenities: strain incompatibilities between neighbouring grains in a polycrystal, stress concentration and distributions in the constituents of composite materials... This corresponds to the goal of *micromechanics* stricto sensu.
- *The computation of industrial components, the size of which is comparable to that of the individual heterogenities.* This situation is met for instance in MEMS for which the grain size can be of the order of magnitude of the sample size, or in critical parts of small components like notches.
- *The prediction of the overall properties of heterogeneous materials.* Homogenization techniques have been designed to bound or estimate the effective properties of materials made of several constituents [2]. Such estimations can be compared with explicit computations of representative volume elements (RVEs) of the material. When the properties of the constituents are highly contrasted and in the case of elastoviscoplastic local behaviour under complex global loading conditions (multiaxial, changes of loading paths, cyclic behaviour...), the latter may well represent the single reliable solution.
- *The simulation of local damage processes.* Damage initiation in heterogeneous materials is not driven by the *mean* values of stress and strain in each constituent, that homogenization methods may be able to estimate, but by some *maximal* values reached at some places of the heterogeneous microstructures (near grain boundaries or interfaces...). The computation of explicit microstructures also provides these local data and can be coupled to damage criteria or damage evolution equations to predict initiation and propagation of damage or cracks.

The continuum mechanical framework sets a lower bound for the relevant scales in the microstructure to be dealt with, namely not below 1 μm in general, especially in the non-linear case (elastoviscoplasticity). The treatment of regions in the material containing a finite number of dislocations definitely falls into the realm of dislocation dynamics [3], which is deliberately excluded from the present study together with similar discrete systems described by explicit schemes. The mechanics of generalized continua however enables one to extend the limits of continuum modelling to lower scales where size effects are expected. The example of a two-phase single crystal superalloy with 0.5 μm cuboidal precipitates, regarded as a two-phase Cosserat medium, is presented in [4]. The introduction of internal length scales in the computation of microstructures is reported in Section 4.2.

Heterogeneous materials generally exhibit a random distribution of phases according to specific statistical distributions so that one single computation will not be enough. Instead a sufficient number of realizations of the microstructure will be necessary to estimate both the wanted property and its dispersion. In particular, the question of the *size of the RVE* for a given geometrical physical property must be addressed.

Microstructural mechanics proceeds in three main steps: representation of the microstructure in a realistic manner, choice of the numerical techniques to solve the boundary value problem and identification of the constitutive equations of the constituents, corresponding to the three main sections of this work. Different types of materials are investigated ranging from two-phase elastic materials to metallic foams, but the stress is laid on the plasticity of crystalline solids. The main example presented in Section 6 deals with the mechanical behaviour of polycrystalline aggregates. Section 7 links the computation of microstructure to the identification of macroscopic constitutive equations for structural applications.

2. Representation of the microstructure

Microscopic observation (optical microscopy, SEM...) usually provides two-dimensional views of the distribution of heterogenities in the microstructure that can be sometimes sufficient to predict the mechanical response of this material element under loading. In the general case, 3D

information should be gathered to reconstruct a realistic representation of the real microstructure.

2.1. 2D and quasi-2D microstructures

The case of thin films or coatings containing grains larger than the sample thickness can be easily handled since 2D characterization gives a thorough representation of the microstructure. Fig. 1 shows an EBSD analysis of a hot-dip zinc coating on galvanized steel sheet [5]. The coating thickness is about 10 μm and the grain size 400 μm. In this case, the EBSD analysis provides a 2D map of the crystal orientation of all grains in the investigated zone, from which the geometry of the grains can be directly inferred. This information can be then used to build a finite element mesh of this microstructure (Fig. 1) for subsequent computations of the mechanical response of the coating. A 2D computation is however not realistic since the deformation mechanisms activated in each grain when the coated sheet is deformed, are highly three-dimensional: basal and pyramidal slip systems have been systematically observed experimentally in the studied zinc alloy which exhibits close-packed hexagonal crystal symmetry. An idealized view of all grains having their *c*-axis perpendicular to the sheet, which may permit a 2D computation, is not acceptable here. Instead, a 3D extension of the mesh in the direction normal to the sheet plane is considered with the minor hypothesis that all grain boundaries are perpendicular to the sheet plane [5].

A similar situation is met in the case of multicrystalline samples for which the grain size is of the order of magnitude of the sample size. A recrystallized sample made of the Inconel 600 alloy and containing six main grains is presented on Fig. 2, after [6,7]. Again a 2D analysis of the problem of the tension of the sample would lead to strong discrepancies with experimental results since the orientations of the individual grains do not display any special symmetry. A simplified 3D representation of the grains can be deduced from the observation of all sides of the sample, as shown on Fig. 2.

2.2. 3D real microstructures

In the general case, the investigated volume contains a large number of heterogenities hidden in the bulk of the materials. The observation of the morphology of individual phases and their distribution in the volume remains a challenging issue, which sometimes remains simply out of reach or requires considerable effort. The polishing and

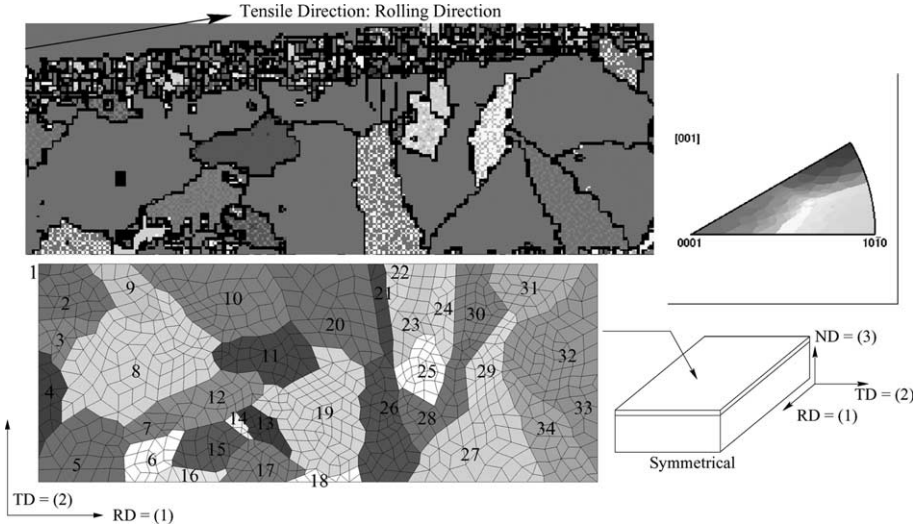

Fig. 1. Grain distribution in a zinc coating on a galvanized steel sheet: EBSD analysis (top); finite element mesh of the grains and 3D extension (bottom); the grain size is about 200 μm on the pictures.

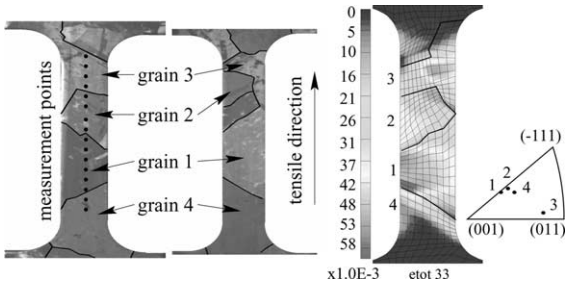

Fig. 2. Multicrystalline nickel sample: both sides of the sample (left), finite element computation and orientation of the grains (right); the gauge length of the sample is about 15 mm.

EBSD analysis of successive layers of a small polycrystalline volume is possible but destructive [8,9].

However, specific techniques are available to image real three-dimensional microstructure in some cases. If the phases of the heterogeneous material have very different densities, *X-ray tomography* can be used. This is the case of metallic foams for instance that have aroused considerable interest in the past 10 years, especially for energy absorption applications [10–12]. A sample of aluminum foam is shown on Fig. 3 with a slice in its interior reconstructed from X-ray tomography [13] and showing a highly heterogeneous distribution of cell sizes.

When one phase of a two-phase material is transparent or can be artificially replaced by a resin transparent to light, *confocal optical microscopy* is a powerful tool to obtain 3D images of the microstructure at least up to a certain depth. It is the case for several materials involved in food industry for instance. The material shown on Fig. 5 is a highly contrasted two-phase material, the elastic properties of the softer phase being more than 1000 less than that of the hard one [14]. The soft phase can be chemically substituted by a transparent resin. Confocal microscopy can be applied providing details on the distribution of the phases in a 50 μm thick sample.

2.3. Random models for microstructures

If three-dimensional images of real microstructures are not available, one can try to simulate them according to some adequate random process. One must then check that the proposed statistical distribution is compatible with information known from 2D observations: volume fraction of phases, two-point correlation functions, morphology (see the corresponding chapters in [15])... Beyond idealized periodic models, such random models exist for instance to describe the structure of metal foams: Voronoi trusses, randomized honeycombs, quasi-periodic beam networks [12]...

The example provided here is the case of polycrystalline morphology presented in detail in [16]. There are two main idealized representations of the polycrystalline microstructure: the periodic model of Kelvin (periodic arrangement of tetrakaideca-

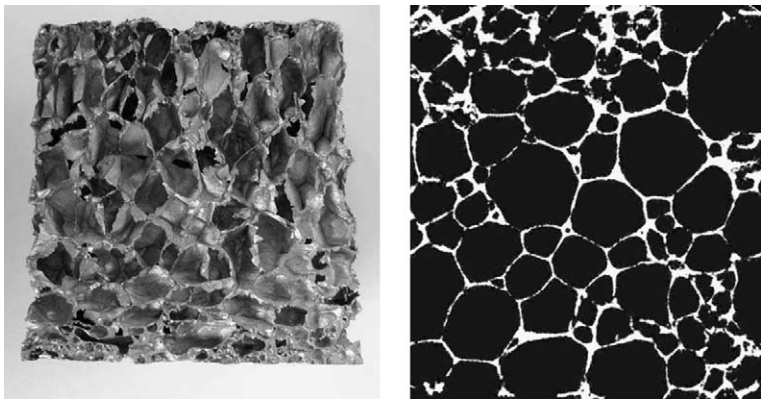

Fig. 3. Cellular morphology of aluminum foams: sample and two-dimension slice reconstructed from X-ray tomography; the edge of the sample is 10 cm long.

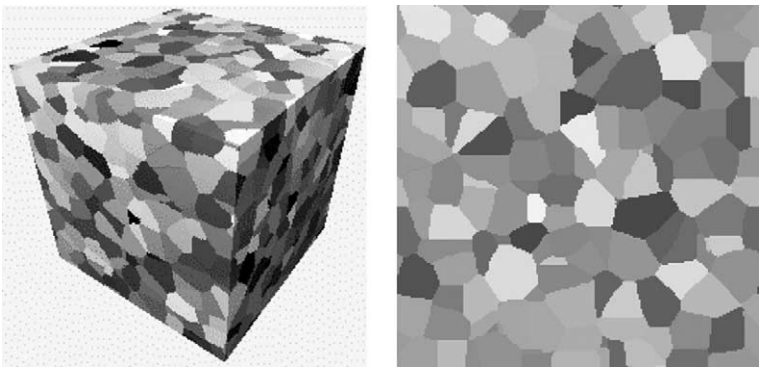

Fig. 4. Simulation of Voronoi polyhedra: 3D distribution (left); section of cube made of Voronoi polyhedra with a periodicity constraint at the boundary (right).

hedra) and the more realistic Voronoi mosaic. One realization of 3D Voronoi mosaic is given in Fig. 4. Once the Voronoi cells have been simulated, a color is attributed randomly to each one. Each color corresponds to a crystal orientation, the prerequisite being that the associated orientation distribution function must be in accordance with the experimental crystallographic texture. In [16,17], isotropic distributions of orientations only have been considered. Note that it is possible to impose a periodicity constraint at the boundary of the polycrystalline cube if one is interested in prescribing periodic boundary conditions in the subsequent computations (see Fig. 4(b)).

2.4. Morphology and mechanical behaviour

The effort dedicated to a realistic and detailed description of the microstructure is all the more important as the morphology can have a drastic influence on the mechanical response of the material, at least if the properties of the constituents are sufficiently contrasted. The example of the two-phase material from food industry represented on Fig. 5 is striking enough to be presented here.

Fig. 5 shows in fact two different morphologies that can be obtained depending on the material processing: one is called here the coarse distribution, the second one the fine morphology. Note that both distributions give the same overall volume fraction of each phase. The elastic properties are highly contrasted since the green/red phase is at least 1000 stronger than the transparent one. The elastic properties of the constituents and of each two-phase materials are measured by means of four-point bending tests [14]. They have been measured as a function of the volume fraction of

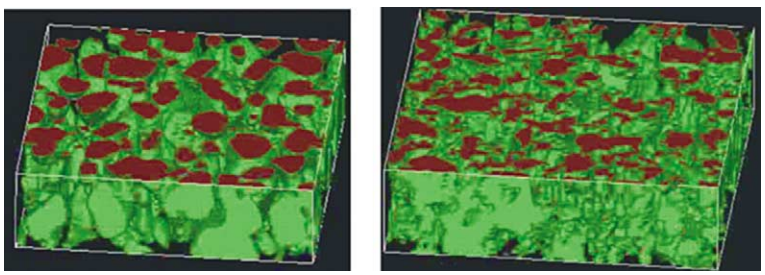

Fig. 5. Three-dimensional microstructure of a two-phase material from food industry obtained by confocal microscopy; the hard phase is represented by the green and red colors: coarse distribution (left), fine distribution (right); the thickness of the layer is 50 μm (after [14]).

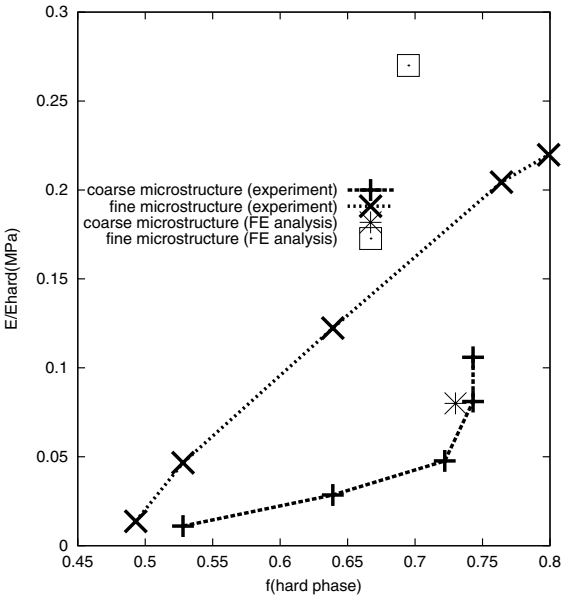

Fig. 6. Mechanical properties of a two-phase material: elastic properties corresponding to the morphologies of Fig. 5 as a function of hard phase volume fraction. Experimental results and numerical estimations for two microstructures.

the hard phase. The experimental results are reported in Fig. 6(a): the fine microstructure turns out to be much stronger that the coarse one. The reason cannot be easily seen from the presented images of both microstructures. One may simply notice that the heterogenities are smaller and more elongated in the fine microstructure than in the coarse one (see also the 2D sections of Fig. 7). When the properties of the constituents are so contrasted, the bounds for the effective properties of the mixture coming from homogenization theory are not really helpful since there is a huge gap between lower and upper bounds. Estimation schemes, like the self-consistent estimate, can then be used to evaluate effective properties. However it is not clear how to decide which approximate scheme is best-suited for each morphology. That is why we propose here to take explicitly the detailed morphology of the presented two-phase microstructures into account and to perform 3D finite element computations. Such a computation of the effective Young's modulus is shown on Fig. 8. This requires a huge mesh and parallel computing. The results obtained for both microstructures are compared to the experimental values on Fig. 6. It can be seen that the full computation makes it possible to distinguish both microstructures whereas the difference of morphology were not easy to assess at a first glance. The localized deformation paths in the soft phase appear clearly in Fig. 8.

3. Numerical techniques

Two main numerical methods are used to solve the boundary value problem for the considered microstructure. The partial differential equations to be solved are the equilibrium equations restricted to the static case in this work. For the computations of RVEs, homogeneous boundary conditions in strain or stress, periodicity condi-

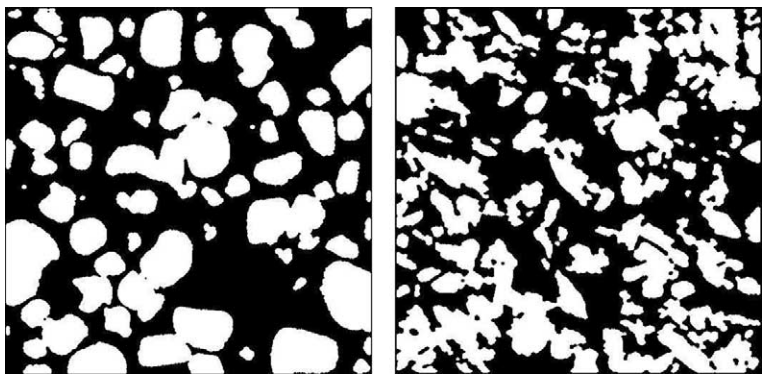

Fig. 7. Two-dimensional slices of both microstructures of Fig. 5.

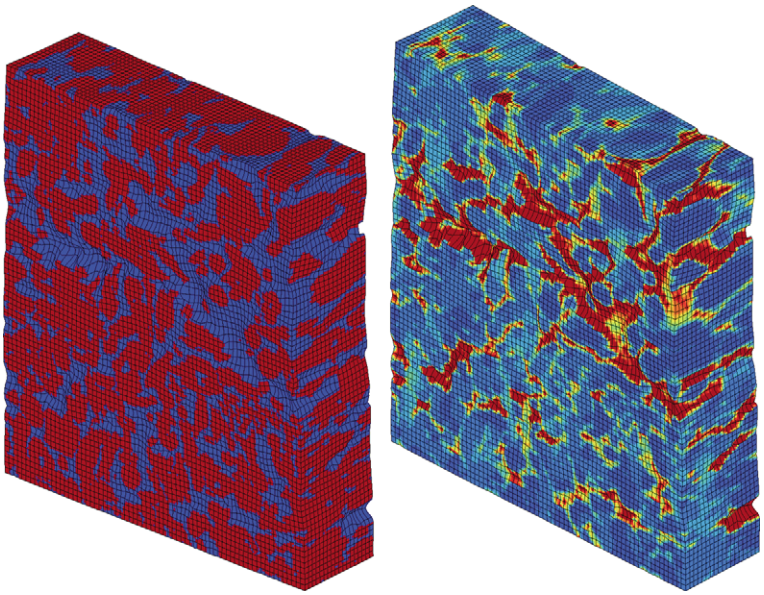

Fig. 8. Three-dimensional finite element simulation of the linear tensile behaviour of a two-phase material: (deformed) finite element mesh of one of the microstructures corresponding to Fig. 5 (left) and field of von Mises equivalent strain (right) for a mean prescribed deformation in vertical direction. The blue/red colors denote low/high strains (88 200 quadratic bricks, i.e. 1 126 131 degrees of freedom, parallel computation on 32 processors).

tions or mixed boundary conditions can be applied at the boundary of the RVE [18]. The finite element method is versatile and has proved to be reliable enough to handle strongly non-linear problems. In the case of periodic boundary conditions, methods based on Fourier transforms have proved to be successful to simulate diffusive or displacive phase transformations [19,20] and, more recently, elastoplastic problems [21]. We refer only to the finite element method in the sequel.

3.1. Meshing microstructures

The choice of the finite element method to solve the considered boundary value problem requires the design of a finite element mesh discretizing the geometry of the microstructure. A straightforward and systematic way, sometimes called *multiphase element technique* consists in superposing a regular 3D mesh on the image of the microstructure. The mechanical property associated with the color of the underlying voxel is attributed to each integration point of all elements (Fig. 9(a)). The drawback of this method is the poor description of interfaces: jumps of some quantities that are in principle allowed at interfaces cannot be described properly if the interface goes through the element. A proper meshing of interfaces is possible in particular in the case of Voronoi polyhedra (Fig. 9(b)) using standard 2D and 3D free meshing techniques [22,23].

A numerical comparison between both meshes of Fig. 9 has been performed for the elastic highly contrasted two-phase material considered in Section 2.4. It shows that the mean values of stress or strain over the whole volume are identical and that the local responses along a given line can differ significantly unless fine enough meshes are used in both cases. This explained why the multiphase element technique is used at several occasions in this and related works.

Similar finite element meshing methods involving Voronoi tessellation can also be found in [24].

3.2. Parallel computing

The obtained three-dimensional finite element meshes usually lead to a huge amount of degrees

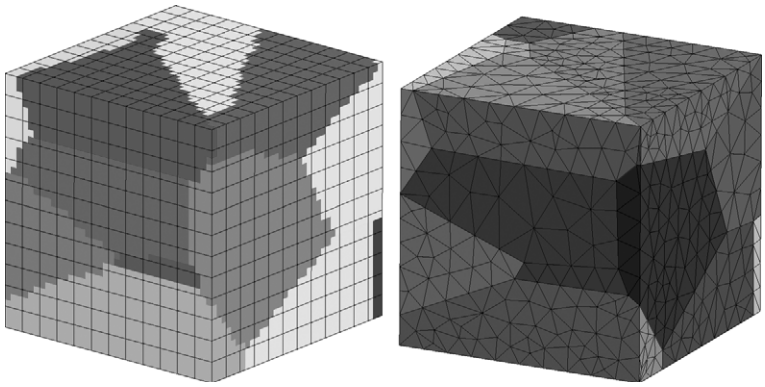

Fig. 9. Meshing 10 Voronoi polyhedra: multiphase element technique (left); 3D free meshing with tetrahedra (right).

of freedom. The resolution of the corresponding linear system requires very large memory and disk storage capacity. On the other hand, it will be seen in Section 4 that the used constitutive equations are strongly non-linear (viscoplasticity, large deformations). The local integration of the evolution equations for the internal variables is very time-consuming. That is why specific resolution techniques are necessary to make it possible to compute realistic microstructures. Parallel computing is a powerful tool introduced in structural mechanics about 15 years ago. At the early stage, independent computation loops were automatically distributed among the processors of dedicated machines. The technology has evolved towards the use of clusters of machines. In the mean time, new computing methods based on subdomain decomposition have been designed. They explicitly take the specificity of the mechanical numerical problem to solve into account, contrary to the previous automatic methods. This lead to a tremendous increase in efficiency.

The parallelized finite element code used in this work [25] resorts to the subdomain decomposition method called FETI [26,27]. It is based on a decomposition of the considered structure into subdomains that can share only interfaces. Each subdomain is handled by one different processor or machine. Parallel solving of local integration of constitutive equations is therefore automatic, provided that the information at an integration point is sufficient for the integration of the variables at this point (local constitutive equations). The subdomains are fixed at the beginning and the problem of dynamic load repartition is not tackled here. At the global level, the independent resolution on a given subdomain leads to discontinuities of the global solution at interfaces. The FETI method is a dual iterative method that tries to distribute the forces at the interfaces for the displacement field to become continuous. One simply mentions here the three main steps of the computation, after the decomposition of the structure into subdomains:

- resolution of the subproblems into each domain;
- iterative scheme to get the solution of the global problem;
- merging the results of all subdomains.

4. Constitutive equations of the constituents

The constitutive equations describing the local behaviour of each constituent in a heterogeneous material definitely are the weakest point in the computation of microstructures. The reason is that the local properties of one phase may differ significantly from that determined on the bulk phase. This is especially the case for non-linear properties like viscoplasticity. One set of constitutive equations is given here for crystalline solids as an example enlightening the anisotropy of local behaviour.

4.1. Crystal plasticity framework

The constitutive theory of crystal plasticity now is a well-established framework to model slip processes at the grain level in a continuum way [28–30]. It is based on the multiplicative decomposition of the deformation gradient $\underset{\sim}{F}$ into elastic and plastic parts:

$$\underset{\sim}{F} = \underset{\sim}{1} + u_{i,j}\underline{e}_i \otimes \underline{e}_j = \underset{\sim}{E}\underset{\sim}{P} \tag{1}$$

where $\underline{u}$ denotes the displacement vector and the $\underline{e}_i$ an orthogonal basis of unit vectors. The choice of the rotation part of the elastic deformation $\underset{\sim}{E}$ is settled by the definition of an intermediate *isoclinic* configuration for which the crystal orientation of the volume element is the same as a reference one. Plastic flow is the results of glide processes according to N slip systems characterized by the slip plane of normal $\underline{n}$ and slip direction $\underline{m}$:

$$\dot{\underset{\sim}{P}}\underset{\sim}{P}^{-1} = \sum_{s=1}^{N} \dot{\gamma}^s \underline{m}^s \otimes \underline{n}^s \tag{2}$$

$$\dot{\gamma}^s = \left\langle \frac{|\tau^s - x^s| - r^s}{K} \right\rangle^n \operatorname{sign}(\tau^s - x^s) \quad \text{with}$$
$$\tau^s = \underline{m}^s \cdot \underset{\sim}{\sigma} \cdot \underline{n}^s \tag{3}$$

A viscoplastic flow rule (3) linking the resolved shear stress τ^s to the increment of plastic slip $\dot{\gamma}^s$ has been adopted. Two hardening variables appear in (3): the threshold r^s called isotropic hardening variable, and the internal stress x^s associated to kinematic hardening. Kinematic hardening at the level of the grains indirectly describes the possible formation of dislocation structures, especially under cyclic loading. The retained non-linear evolution rules are the following:

$$r^s = r_0 + Q\sum_{r=1}^{N} h^{sr}(1 - \mathrm{e}^{-bv^r}), \quad \dot{v}^s = |\dot{\gamma}^s| \tag{4}$$

$$x^s = c\alpha^s, \quad \dot{\alpha}^s = \dot{\gamma}^s - d\dot{v}^s\alpha^s - \left|\frac{x^s}{M}\right|^m sign(x^s) \tag{5}$$

The initial plastic threshold is r_0 and h^{rs} denotes an interaction matrix accounting for self and latent hardening. The evolution equation for kinematic hardening contains dynamic and static recovery terms. Note that other choices of hardening variables are possible, for example dislocation densities-like variables appearing in some evolution rules used in physical metallurgy [31,30]. Most of them however do not significantly differ from the responses obtained using Eqs. (3)–(5).

The material parameters appearing in the constitutive equations have been identified for instance in the case of single crystal copper or nickel-based superalloy under tension, cyclic loading and creep [32,33]. Even though the form of the constitutive equation is still pertinent to describe the behaviour of a grain in a polycrystal, the values of the parameters may differ for the bulk single crystal and the grain in a polycrystal, because of grain size effects for instance. The values of the parameters for the grain are usually identified from an inverse approach using the overall mechanical response of the polycrystal and a polycrystal homogenization model. The bias introduced by the choice of a specific simplified homogenized polycrystal model sheds some dark on the relevance of the found local parameters. In particular, very different values can be found to describe the same global curves if a Taylor or a self-consistent model is used [1]. The use of the obtained constants for the simulation of the polycrystalline aggregates computed in Section 6 is then questionable. A first attempt of a direct inverse approach based on polycrystalline aggregates is reported in [34].

4.2. Introduction of a length scale

The aim of the mechanics of heterogeneous materials in the case of metal polycrystals should be to predict the polycrystal behaviour from the knowledge of a constitutive model for the single crystal, the crystallographic texture and the grain morphology. This procedure fails due to the fact that the proposed framework is up to now insensitive to the influence of grain size classically observed in metallurgy [35]. It must be noticed that within the classical continuum mechanical framework the absolute size of heterogenities in the materials of Fig. 6(b) or 9 does not play any rôle in the final local and global responses. There is no effect of the absolute dimension in the coordinates of the nodes in the mesh.

Therefore a more realistic microstructural mechanics should be able to put a scale on the strain maps of Fig. 11, as in the corresponding micrographs. The introduction of explicit metallurgical rules like the Hall–Petch correlation cannot be used inside the grain since they are valid for the macroscopic response only. A solution to this difficulty is to introduce additional hardening variables incorporating an intrinsic length scale. One of them is the so-called *dislocation density tensor* (also called density of geometrically necessary dislocations) defined as the rotational part of the inverse of the elastic deformation [36]:

$$\underset{\sim}{\alpha} = -\underset{\sim}{\mathrm{curl}}\underset{\sim}{E}^{-1} \tag{6}$$

that has the dimension of the inverse of a length. The meaning of this quantity is made clearer when it is related to the lattice curvature tensor $\underset{\sim}{\kappa}$. Lattice rotation connects an initial reference crystal orientation of a single crystal element to its current orientation. It is therefore related to the rotation part in the polar decomposition of $\underset{\sim}{E}$. As a rotation, it can be represented by an axial vector and, at least in the small rotation framework, the gradient of it is the definition of lattice curvature $\underset{\sim}{\kappa}$. Lattice curvature can be deduced from EBSD maps of a deformed crystal. It is usually postulated that lattice curvature contributes to material hardening [37], for instance according to

$$r^s = r_0 + Q\sum_{r=1}^{N} h^{sr}(1 - \mathrm{e}^{-bv^r}) + H\theta^s \tag{7}$$

where θ^s denotes a lattice curvature angle over a given length scale. This enhancement of the classical crystal plasticity framework falls into the mechanics of generalized continua, since it has been incorporated in strain gradient or Cosserat formulations of continuum mechanics [4,38]. It has been shown to provide Hall–Petch like grain size effects on polycrystal behaviour in the case of f.c.c. and h.c.p. materials [4,39]. The generalized continuum affects also the obtained strain localization modes at stress concentration points or cracks [40].

4.3. Coupling with other physical mechanisms

Dislocation glide processes are not always the single physical mechanism at work in a plastically deformed materials. Other deformation and damage modes should be included: deformation twinning, stress-induced phase transformation, recrystallization, trans or intergranular cracking... Fig. 10(a) shows a 2D simulation of intergranular cracking in a zirconium alloy [41]. In Fig. 10, the grains boundaries have a non-vanishing thickness in order to attribute specific properties to them: intergranular viscous sliding or damage observed at high temperatures. In [41,42] the mechanical framework is coupled to diffusion processes in a weak formulation, to predict stresses due to the growth of oxide layers on the one hand, and stress assisted corrosion.

Several of these important physical mechanisms can be simulated individually. However they often act simultaneously or concurrently and the main

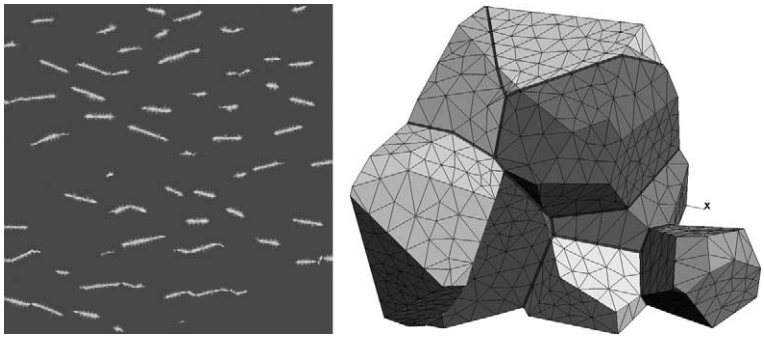

Fig. 10. Modelling intergranular damage in a polycrystalline aggregate: damage initiation in two-dimensional polycrystal under vertical tension (left); 3D meshing of damageable grain boundaries (right).

difficulty for future computations will be to cope with the increased non-linearity of the coupled problems.

5. Computation of multicrystals

The interest of computing samples containing a small number of large grains lies in the fact that the whole framework can be checked experimentally by comparing local and global predictions to strain or stress field measurements. In the case of coatings for instance, the computations are also of industrial interest since they can be used to optimize the microstructure, like grain size for instance.

5.1. Multicrystalline specimens and coatings

Metallic multicrystals have been investigated both experimentally and numerically in several situations in the past 10 years: copper bicrystals [33], copper, nickel, aluminum or iron multicrystals [6,43–45]. The specimens may be strained in situ in a SEM. An EBSD analysis provides the lattice rotation field and the use of grids on the surface enables one to derive some components of the strain fields. In all mentioned contributions, the experimental results have been compared with success with realistic 3D computations using crystal plasticity.

The application of the methodology to metallic coatings is perhaps more important from the industrial point of view. The case of zinc coatings on steel sheets has been presented in Section 2.1. The finite element computation of the tension or expansion of a coating on its substrate using the mesh of Fig. 1 for instance, reveals the following features of the coating behaviour:

- the multiaxial stress state of each grain depending on its orientation;
- activated slip systems in the core of the grains, at the grain boundaries and at the interface coating/substrate;
- the gradient of strain that can develop from the interface to the free surface; this gradient can be shown to increase when the ratio between in-plane grain size and coating thickness decreases;
- forces acting at grain boundaries and at the interface, that can lead to intergranular fracture or interface decohesion;
- the coating roughness induced by local plasticity.

A detailed illustration of these points can be found in [5].

5.2. Confrontation with strain field measurements

The results of the previous calculations can be directly compared with experimental strain field measurements giving a distribution of some mechanical or physical quantity generally at the surface of the specimen:

- Total strain field measurements using a fiducial grid technique; the grid is deposited on the surface of the sample by electrolithography with a step ranging from 1 to 10 μm or more (see [46] and several contributions in the same volume). Comparisons between simulation and measurement are provided in [43,44] for multicrystalline aggregates. The agreement can be improved using refined meshes and accurate 3D grain shapes. If the surface exhibits a sufficient roughness, the grid is not necessary any more and image correlation analysis can be used to estimate the strain field from one image to the other. This is the case for metal foams for instance [12].
- Lattice orientation field measurements by EBSD provide not only the relevant distribution of grain orientation to be used in the simulation of multicrystals but also its evolution during deformation. The lattice curvature field can be deduced from this information. The crystal plasticity models are able to predict such orientation changes due to plastic slip (confrontation between simulation and measurements in [46] and [7] for instance).
- Elastic strain field measurements by X-ray local measurements; they are usually translated into stress maps relying on elastic constants. Stress heterogenities from grain to grain or stress distribution in a large grain can be determined and have been compared with FE computations [7]. More ambitiously, the X-ray imaging technique

using the synchrotron facility of HASYLAB in Hamburg—Germany, gives a complete image of the elastic deformation and lattice orientation distribution in a given grain. A complex image data treatment is necessary [47].

6. Computation of polycrystalline aggregates

The type of geometrical aggregates shown in Fig. 4 can be used to investigate the intragranular fields, and to contribute to a better knowledge of the state of stress and strain in a current point of a polycrystal, and in more critical areas like the vicinity of the surface or at the grain boundaries. To be significant, the calculation must involve a reasonable number of grains *and* a reasonable number of elements in each grain. According to the literature related to texture effect, 1000 of grains seems to be a good number for representing a given material. The following examples are restricted to 200 grains, in order to have more than 1000 integration points in each grain ($10 \times 10 \times 10$, in 3D). Averaged values can then be considered on the mesh, in order to compare the FE model to the results given by more simple models like self-consistent approaches, on the level of each grain, and for the global mechanical response. The elements used are 20-node bricks with 27 integration points per element.

6.1. Boundary conditions and representativity of the volume element

Five types of boundary conditions will be considered on a cube containing 200 grains:

- Homogeneous strain boundary conditions (labelled HSB): the three components of the displacement at each node of the outer surface are prescribed according to the equations:

$$u_i = E_{ij} x_j \tag{8}$$

  where $\underset{\sim}{E}$ is a given constant strain tensor and $\underline{x}$ the position of the point. We apply in this work a strain $\underset{\sim}{E}$ corresponding to average uniaxial tension. The values of the component are taken from a simulation with a homogenized polycrystal model;
- Mixed boundary conditions (labelled MB) for which only the displacement normal to the surface is prescribed according to the previous equation;
- Tension with one free surface (labelled 1FF): the same as MB except for one face of the cube which is let free of forces;
- Tension with four free faces (labelled 4FF): normal displacement is zero at the bottom and prescribed at the top. The four lateral faces of the cube are free of forces.

In the whole section, the local and global behaviour of the polycrystal is investigated. No special property is attributed to the grain boundaries. In particular, grain boundary sliding or damage are not considered in this section.

The representativity of the considered polycrystalline volume element is an essential issue. The number of grains must be large enough for the volume to be sufficiently representative. On the other hand, the number of elements inside each grain must be large enough for a sufficiently accurate description of the local intragranular strain field. That is why the presented computations belong to the largest computations of polycrystals available in literature and require parallel computing. With the number of processors used, the compromise is a volume containing 200 grains. The representativity of the volume element depends on the contrast of phase properties, on the type of boundary conditions and on the wanted accuracy of the estimation of the effective property [48]. It can be assessed by applying strain based and stress based boundary conditions on the same volume [49]. The difference between the apparent properties found for both conditions is due to the lack of representativity of the sample. For large volumes, the choice of the boundary conditions should not matter any more. The tensile curves obtained for both conditions on the considered sample of 200 grains differ by about 6%. The tensile curves can be found in [17]. This difference can also be seen in Fig. 13. The attention is now focused on the intragranular fields.

6.2. An approach to intragranular fields

Fig. 11 shows respectively the von Mises equivalent stress on a 12^3-mesh (a), on a 18^3-mesh (b), on a 32^3-mesh (c), then the grain map (d), and finally the total amount of plastic slip (sum of the slip on all the slip systems) for the 18^3-mesh (e) and for the 32^3-mesh (f). For each plane, ξ is the distance to the center of the aggregate normalized by its half width a, $\xi = x_1/a$. The material is IN600 [17], the cube is submitted to a 1.5% overall tension, and the orientations of the grains are randomly distributed, in order to simulate an initially isotropic material. The 12^3-mesh is obviously

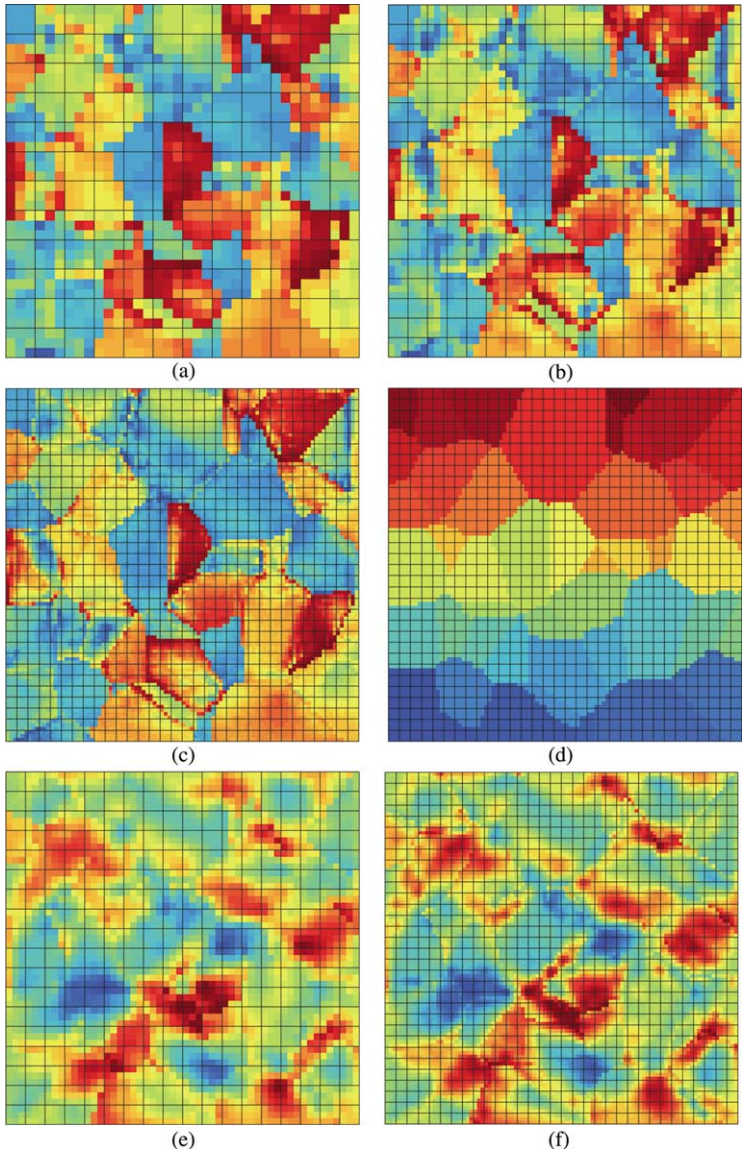

Fig. 11. Contour plots for the Gauss points near ($\xi = 0$) for a tension test along x_3-axis: von Mises stress in 12^3-mesh ($\xi = 0.08375$) (a), 18^3-mesh ($\xi = 0.09875$) (b) and 32^3-mesh ($\xi = 0.09375$) (c); (d) grain map in 32^3-mesh, amount of plastic slip in 18^3-mesh ($\xi = 0.09875$) (e) and in 32^3-mesh ($\xi = 0.09375$) (f).

much too crude to correctly represent the local fields. The global variations are generally captured, but the finely heterogeneous areas near the grain boundaries are absent of the contour plot. The 18^3-mesh is a little better, especially for the von Mises stress, which is well predicted far from the grain boundaries since it is rather uniform inside each grain. But it is not the case for the amount of plastic slip: there are some grains where high-slip-activity-structures form near grain boundaries and where the rest of the grain remains unaffected by slip activity. Such features are strongly dependent on the resolution of the mesh near the grain boundary: if the 18^3-mesh only is considered, one may observe high-slip-activity-regions spreading over grain boundaries. But with a higher resolution, these structures appear to be disconnected at the grain boundaries, thus illustrating the fact that for the present case, the slip activity is mainly due to the gradients of stress at the grain boundaries and not related to a kind of propagation of slip across boundaries.

Hence, having about $3 \times 3 \times 3$ quadratic elements per grain (case of 18^3-mesh) may lead to a first good estimation of the gradients of the fields inside grains. Yet, for a systematic treatment aiming at describing the effect of grain boundaries (e.g. plotting field variables vs. the distance to the grain boundary and averaging over the grains of the aggregate), the uncertainty resulting from the fact that grain boundaries pass inside elements instead of between elements (so-called multiphase elements) could alterate the observations made in the vicinity of the boundaries. Such a systematic treatment requires to have at least $4 \times 4 \times 4$ elements per grain so that one is sure that there are $2 \times 2 \times 2$ single-phase elements inside each grain, i.e. enough elements unaffected by the numerical construction of grain boundaries.

The heterogeneity of the local fields can also be studied by plotting stress–strain curves. The result is shown in Fig. 12, for the biggest grain (number 58) and the strongest grain, presenting the maximum axial stress (number 132) in the aggregate. The graphs in Fig. 12(a)–(d) are obtained with homogeneous strain boundary conditions (HSB). For the biggest grain, the mean behaviour is close to the single crystal response (the response of an unique grain having the same orientation, and tested under the same macroscopic strain), and a large scatter is present. This scatter remains even if the first integration points close to the grain boundaries are removed from the picture. It should be noted also that the stress redistribution induces some local unloadings. As illustrated by Fig. 12(b), the various points in the grain are located in the $\sigma_{33} - \sigma_{11}$ axial stress–lateral stress plane on a line like $\sigma_{33} - \sigma_{11} = C^{te}$. There is a fluctuation of the hydrostatic pressure more than a change in the deviatoric components (the same plot would be obtained for σ_{22}). For grain58, the two branches of the graph are balanced, so that the average lateral stress is about zero. This is not the case for grain132. This grain is smaller, and it is strongly overloaded by its neighbours, so that the local σ_{33} stress is far larger in the aggregate than in the relevant single crystal (Fig. 12(c)) and an important lateral stress is observed, since the segment in the $\sigma_{33} - \sigma_{11}$ plane is no longer symmetric with respect to σ_{11}-axis. The large variation on hydrostatic pressure predicted by the FE model could not be seen by a mean field model, since in this case the elasticity is assumed to be uniform. On the other hand, it is not surprising to check that hydrostatic pressure strongly depends on the boundary conditions. As shown in Fig. 12(e) and (f), the overloading effect on grain132 vanishes for the same aggregate computed with four free lateral faces (4FF).

6.3. Comments on the surface effect

Opposite results can be read in the literature concerning the effect of a free surface on local plastic behaviour [50]. After extensive TEM studies, some authors [51] observe a hardened surface, due to the increase of dislocation density, but other works [52,53] display an inverse effect, with lower dislocation densities and larger cell sizes. On the other hand, attempts have been made to approach the surface effect from a mechanical point of view, using a crystallographic inclusion in a homogeneous semi-infinite medium, considered as elastoviscoplastic [54] or just elastic [55]. In both cases, the authors find that surface relaxes the stress level, the perturbed area corresponding to

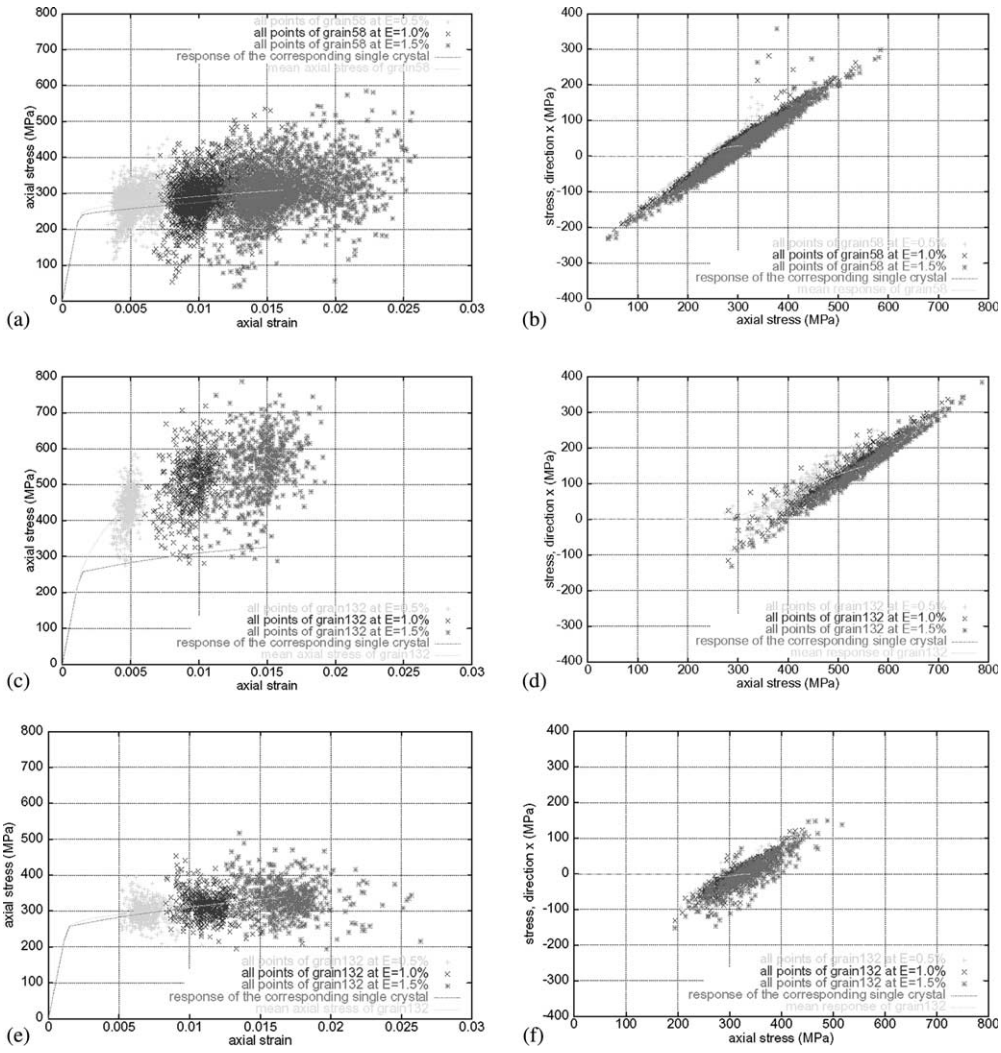

Fig. 12. Illustration of the low (a,b), (e,f) or high (c,d) grain-to-grain interaction for three levels of macroscopic strain ($E = 0.5\%$, 1.0%, 1.5%), with homogeneous strain boundary conditions (HSB) or four free faces (4FF) (a) σ_{zz} vs. ε_{zz}, grain58 (HSB), (b) σ_{xx} vs. σ_{zz}, grain58 (HSB), (c) σ_{zz} vs. ε_{zz}, grain132 (HSB), (d) σ_{xx} vs. σ_{zz}, grain132 (HSB), (e) σ_{zz} vs. ε_{zz}, grain132 (4FF), (f) σ_{xx} vs. σ_{zz}, grain132 (4FF).

about three grains. Without repeating here the discussion of this problem, which can be found elsewhere [17], a summary of the main results is now given. Having real neighbours instead of a homogeneous medium changes everything for each grain, so that the first order surface effect is *scatter*:

- as described in Fig. 12, relaxing the boundary condition can produce a drop of the local stress, but in some other location, a very low stress level obtained with HSB boundary conditions can increase when freeing the surface;
- there is a a lower difference between 4FF and MB (a mixed case with just imposed normal displacement on the lateral faces but free in-plane) than between MB and HSB;
- averaged quantities can be considered, by plotting the average value of a critical variable in a

slice at a given distance of the free surface. In that case, the observed effect is small. For instance, it is shown in Fig. 13 that the boundary conditions have an effect on the mean value of the von Mises stress (that demonstrates that the cube is too small to be a mechanical RVE), and, on the other hand, the stress drop that can be attributed to the surface effect is significant (relative value of about 10%). Some other typical variations are reported in Table 1. At the surface of the cube:

- the number of active slip systems is significantly smaller (more than 15% less than in the middle of the specimen), then the sum of the plastic slip is also smaller;
- on the other hand, the slip systems are "more efficient", the maximum amount of slip is larger, and finally the equivalent von Mises strain is larger too.

6.4. Effect of the grain boundary

Returning to the grain58 already observed in Fig. 12, we plot the values of the axial stress and axial strain vs. the distance to the grain boundary. The first Gauss point belonging to the grain receives a value of zero, and the Gauss points in the middle of the grain have the largest distance, of about 2.5, that means that the grain "diameter" is about 5 (to be compared with 18, which is the

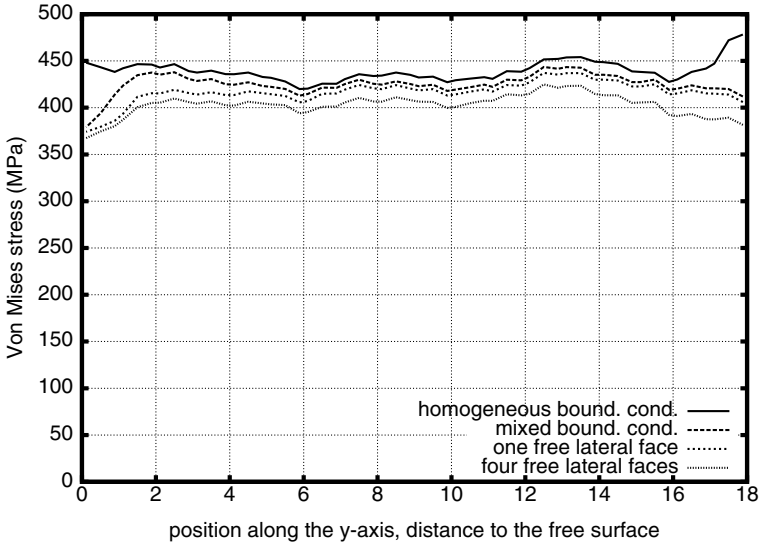

Fig. 13. Illustration of the surface effect on the von Mises stress for various boundary conditions. Dimension of the cube = 18, free surface in $x = 0$ (1FF), in $x = 0$ and 18 (4FF).

Table 1
Effect of the boundary conditions on several variables; the average is given in each box, together with the relative local variation in ($x = 0$)

	von Mises stress (MPa)	von Mises strain	Sum of plastic slips	Max amount of slip	Number of systems with slip >0.001
HSB	438 (+2.5%)	0.0144 (−4.6%)	0.0345 (+3.5%)	0.0151 (−3.0%)	4.30 (+4.5%)
MB	422 (−11.2%)	0.0147 (+3.6%)	0.0338 (−5.3%)	0.0160 (+7.6%)	3.83 (−16.7%)
1FF	415 (−11.3%)	0.0148 (+3.5%)	0.0333 (−5.1%)	0.0162 (+7.7%)	3.73 (−19.8%)
4FF	405 (−9.7%)	0.0148 (+3.5%)	0.0323 (−3.1%)	0.0167 (+7.6%)	3.56 (−16.7%)

actual size of the present mesh). Like the surface, the grain boundary will first produce a large scatter, in terms of stress and strain. The average values are also drawn for the two curves, the axial strain increases at the center of the grain, but the stress is almost constant (Fig. 14).

If some other grains are considered, the dispersed character of the mechanical fields remains present. On the other hand, in order to determine a general rule, averaged values were also taken [56], so that the resulting curves show the chosen variables in each grain as a function of the absolute distance to the appropriate grain boundary. The von Mises stress is taken in Fig. 15 to illustrate this type of plot. The stress increases a little bit at the grain boundary, but it is difficult to discriminate between a real, physical increase, and the artefact related to the poor description of the displacement field in this area. On the other hand, the stress tends to decrease in the middle of the grain. By the way, the biggest grain (grain58) is known to show very low values. To summarize the other types of plots, one has to remember that:

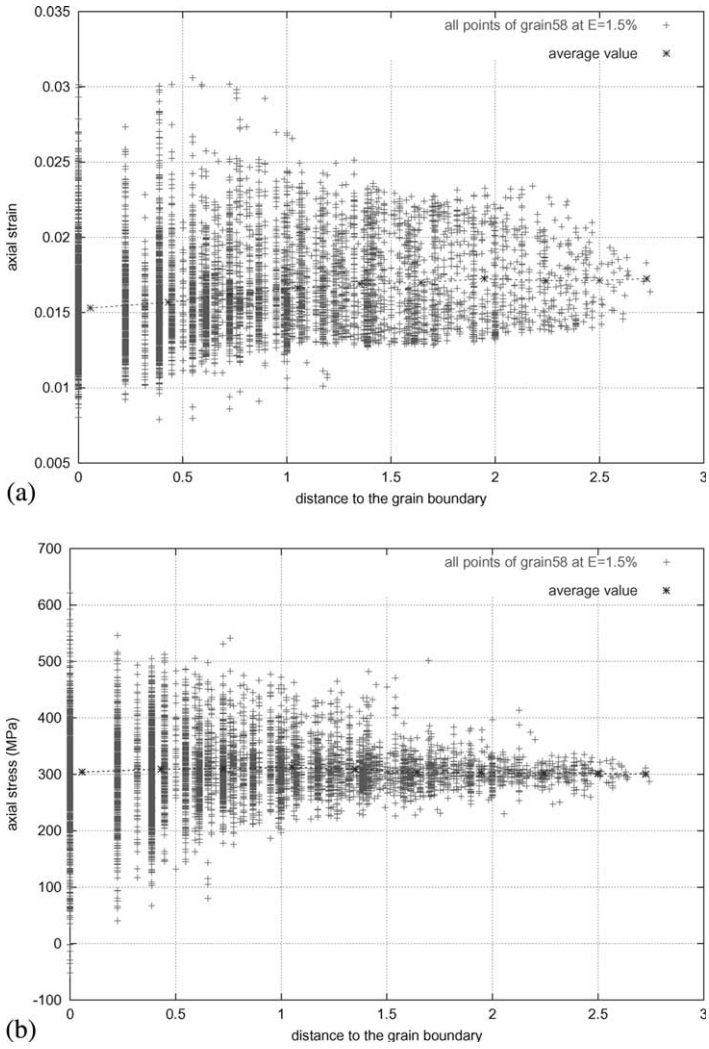

Fig. 14. Effect of the grain boundary in grain58, (a) axial strain, (b) axial stress.

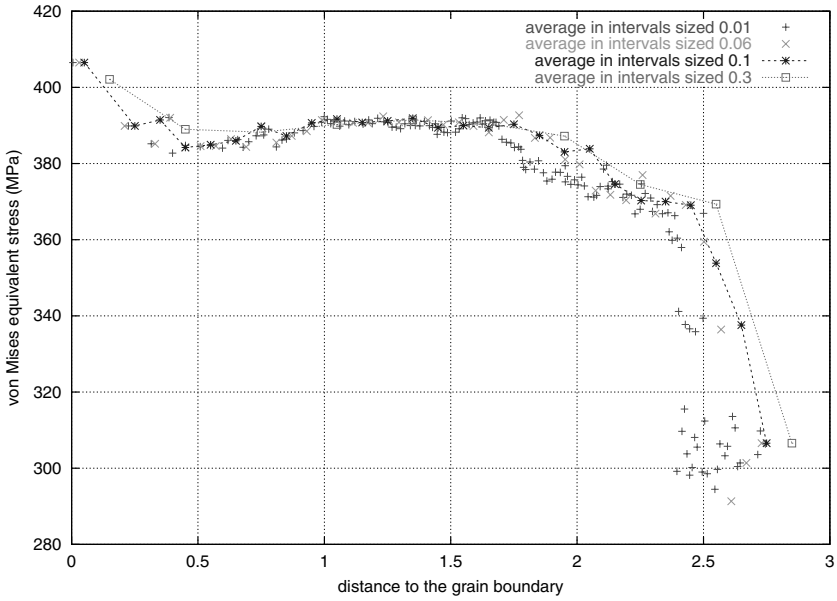

Fig. 15. Effect of the grain boundary on von Mises stress for all the grains in the aggregate.

- the number of active slip systems increases near the grain boundary;
- the sum of the plastic slips increases near the grain boundary;
- the von Mises strain is larger in the center of the grain;
- the von Mises stress is smaller in the center of the grain.

The situation is quite different in the case of an aggregate of h.c.p. crystals like zinc. For this class of symmetry, elasticity and plastic slip are strongly anisotropic. In the zinc alloy studied in [5,34], the activated slip system families are mainly basal slip and pyramidal Π_2, the latter having an initial CRSS 10 times bigger than the former. The consequence is that pyramidal slip takes place principally near the grain boundaries whereas basal slip spreads over the entire grain.

7. Identification of scale transition rules and link with macroscopic constitutive equations

The results of the previous section demonstrate that the local fields present very strong gradients within the grains. The purpose of the present section is now to evaluate the response of the mean field models with respect to these solutions. Even if these models cannot produce a detailed description of the intragranular fields, they might be able to approach the response averaged on grains having the same orientation. We first give a brief description of these models, then show the results.

7.1. Scale transition rules for the polycrystal

In a polycrystalline aggregate, one phase may be characterized by its shape, volume fraction, crystallographic orientation, location with respect to the surface of the material, etc... Most of the models usually specified for polycrystals made of equiaxial grains retain only the crystallographic orientation [57–59], and put in the same *crystallographic phase* all the grains having the same orientation. Thus the alloy is considered as a *n*-phase material, each phase being defined by a set of Euler angles, and then the model is used to describe the mean behaviour of all of them.

The relation (9) summarizes the results given by several homogenization polycrystal models, ac-

cording to the definition of α, with a specific mention to $\alpha = 2$ [60] representing uniform total strain, to $\alpha = 1$ [61], corresponding to an elastic accommodation of the homogeneous equivalent medium, or to (10) involving the overall equivalent stress Σ in uniaxial tension and the equivalent plastic strain p deduced from the overall plastic strain tensor $\underset{\sim}{E}^{\mathrm{p}}$ [62]. This last model is the simplified expression extracted from the general self-consistent model due to Hill [63], valid for isotropic elasticity and radial loading paths.

$$\underset{\sim}{\sigma}^g = \underset{\sim}{\sigma} + \mu\ \alpha(\underset{\sim}{E}^{\mathrm{p}} - \underset{\sim}{\varepsilon}^{\mathrm{pg}}) \tag{9}$$

with

$$\frac{1}{\alpha} = 1 + \frac{3\mu p}{2J_2(\Sigma)}, \quad p = \left(\frac{2}{3}\underset{\sim}{E}^{\mathrm{p}} : \underset{\sim}{E}^{\mathrm{p}}\right)^{1/2} \quad \text{and} \quad \underset{\sim}{E}^{\mathrm{p}} = \langle \underset{\sim}{\varepsilon}^{\mathrm{pg}} \rangle \tag{10}$$

From a physical point of view, the previous rules simply show that local plastic strain reduces the local stress, whereas the stress redistribution related to plastic accommodation tends to decrease for larger plastic strains. An alternative formulation, the "β-model", introducing a non-linear accommodation, has also been proposed [64]. It can be calibrated from finite element computations, using either an inclusion embedded in a homogeneous medium [65] or a 3D FE polycrystal [34]:

$$\underset{\sim}{\sigma}^g = \underset{\sim}{\sigma} + \mu(\underset{\sim}{\beta} - \underset{\sim}{\beta}^g) \quad \text{with } \underset{\sim}{\beta} = \sum_g f^g \underset{\sim}{\beta}^g \tag{11}$$

Various expressions can be used for the evolution of the variable β^g in each grain [18]. The model can be used for any kind of loadings, especially cyclic loadings.

7.2. Stress–strain behaviour of the grains

The mean values predicted by the mean field models present a lower dispersion than the FE results. Fig. 16 shows the curves obtained with the model proposed in [62] (BZ) (a) for a tension until 1.5%. As expected, for the final state, all the points are on the same line, the slope of which is −22 000 MPa, showing that the accommodation is elasto-

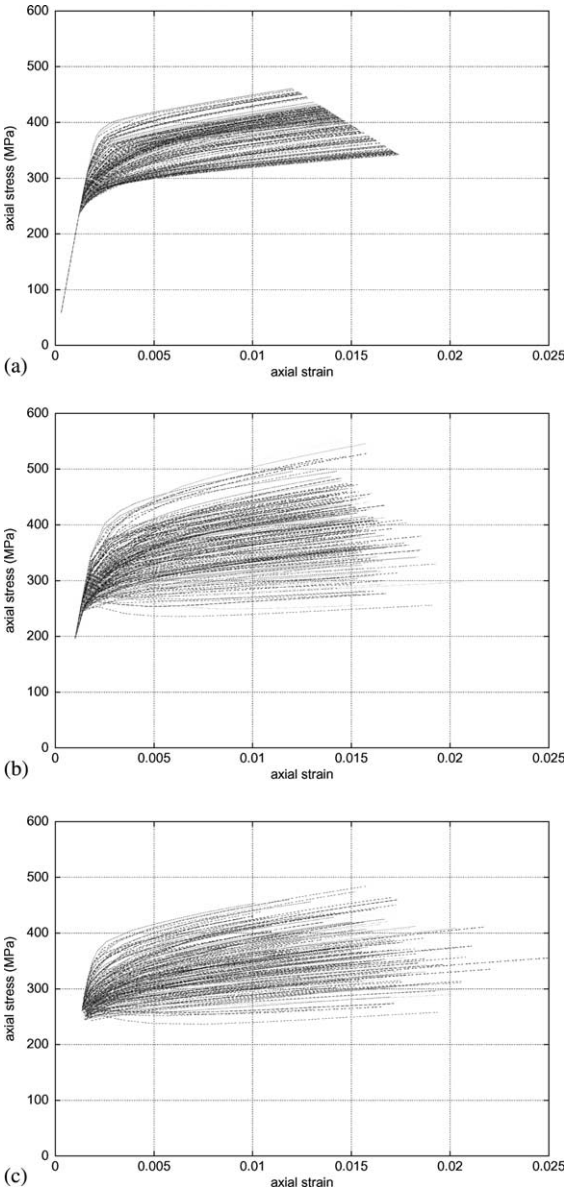

Fig. 16. Axial stress–strain curves of the 200 grains of the aggregate, (a) Berveiller–Zaoui model, (b) cube, HSB, (c) cube, 4FF.

plastic. The stress range is about 115 MPa between the softest grain and the strongest one and the strain range about 0.5%. The results from FE computations are given in Fig. 16(b) for a HSB case, and Fig. 16(c) for the 4FF case. The stress redistribution due to the local fields no longer

respects the nice rule coming from the self-consistent approach, and it is even difficult to extract a relation between local stress and local strain. At least, one can check that a fully constrained type of load dramatically increases the scatter on stress (range of 294 MPa), but the strain range is also larger than with the BZ model (0.86%). On the other hand, the stress range is smaller for the 4FF case (range of 230 MPa, but still two times bigger than with BZ model), but the strain values are now very dispersed (range of 1.5%).

The local grain-to-grain interactions seem to play a very important rôle in the stress redistribution. This fact is also illustrated in Fig. 17, which shows the grain response in the $\sigma_{22} - \sigma_{33}$ (lateral stress vs. axial stress) plane. Since the grain elasticity was chosen isotropic, all the grains are equivalent up to the onset of plasticity, for $\sigma_{22} = -74$ MPa and $\sigma_{33} = 148$ MPa. Then, the plastic flow produces contradictory evolutions according to the grain: the lateral stress can either increase or decrease, and the stress paths are non-proportional.

A final view of the difference between FE and mean field models is given in Fig. 18, which shows a plot of the mean axial stress in several grains according to different calculations, along a line located near the middle of the cube, perpendicular to the tensile direction. For each grain, the figure shows:

- the result obtained in the single crystal having the same orientation;
- the result obtained with the BZ model;
- the results obtained with various meshes, from 10^3 to 32^3 elements.

The stress levels predicted by the BZ model are larger than the single crystal results (one could also have lower values). Again the dispersion observed for all the FE computations is larger than the dispersion of the self-consistent approach.

However, this comparison is not definitive because of the lack of representativity of the considered sample in terms of number of grains of close orientation. Accordingly, the comparison must be drawn again in the future for larger aggregates.

8. Conclusions and prospects

Microstructural mechanics lies at the junction between structural mechanics and material sciences. It has been illustrated for two main types of applications:

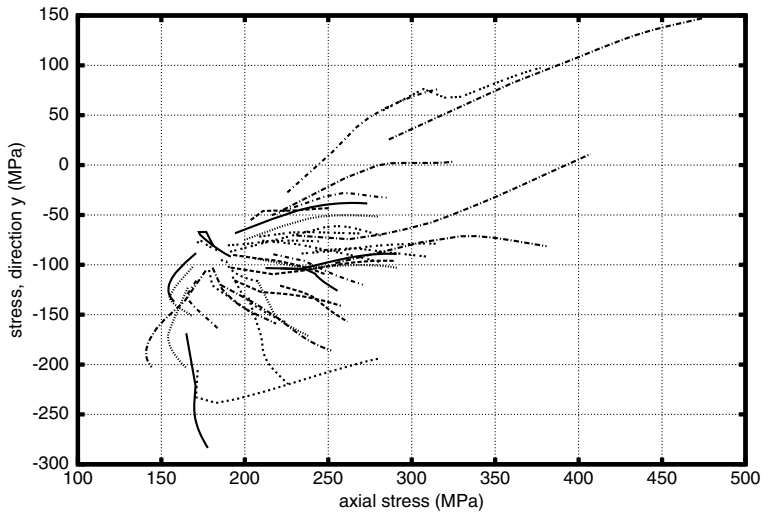

Fig. 17. Mean stress paths in each of the 200 grains of the aggregate after 1.5% tension.

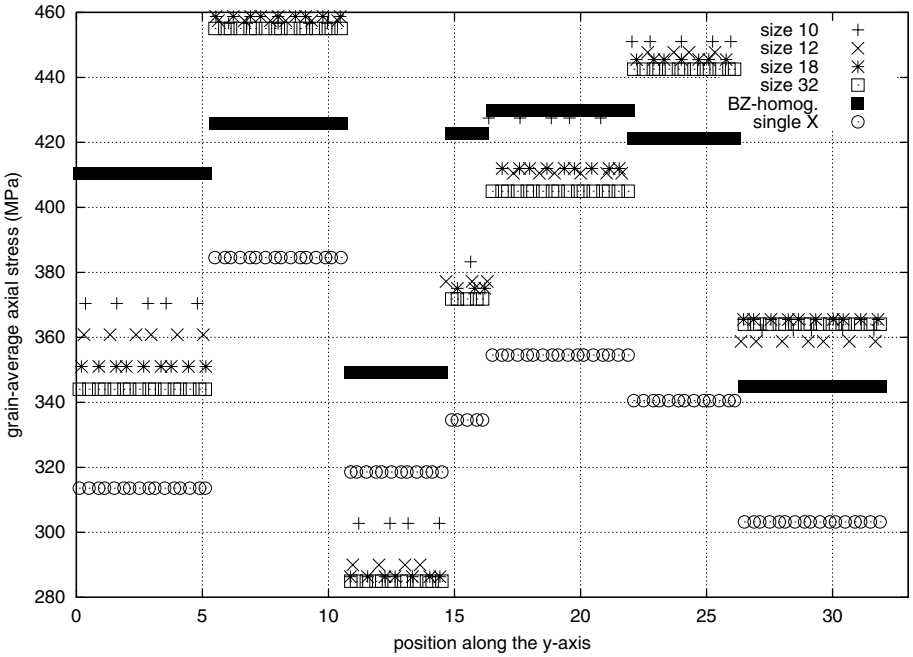

Fig. 18. Mean axial stress in grains located along a line crossing the aggregate: mean stress per grain from four different sizes of mesh (10^3, 12^3, 18^3, 32^3 elements), stress from the homogenization model, stress in the corresponding single crystals.

- Computation of specimens or industrial components for which the size of the heterogenities of the material is of the order of the size of the structure or of its parts (holes, notches...). Examples are films, coatings, MEMS, sensors, multiperforated blades or combustion chambers...
- Computations of RVEs of random heterogeneous materials, with a view to predicting overall properties and optimizing microstructures (morphology, size...).

In both cases, realistic three-dimensional computations are necessary. Parallel computing seems to be the only possible solution to perform them (on networks of standard PCs). The simulations of polycrystalline aggregates for instance show the tremendous heterogeneity of stress and strain fields within grains that cannot be predicted by available explicit homogenization models. Such stress and strain concentrations may well be the precursor of crack initiation and growth.

Regarding computational homogenization methods, the notion of RVE is essential and remains to be defined properly. Its size depends on the studied property (thermal, mechanical...), on the contrast of properties between the constituents, on phase morphology and on boundary conditions. If the contrast is very high, a RVE may contain a considerable number of heterogenities, which makes the computation untractable. Smaller sizes can however be used provided that a statistical treatment of a sufficient number of realizations of the microstructure is considered [66,48]. A first approach of the size of RVE for polycrystals can be found in [67]. Other applications dealing with fiber or particle composites should be considered.

The next step will be the systematic use of such techniques to simulate damage and fracture of heterogeneous materials under complex thermomechanical loading conditions. Considerable numerical difficulties will arise due to the high nonlinearity of the problem associated with strain and damage localization phenomena.

References

[1] E. Sanchez-Palencia, A. Zaoui, Homogenization techniques for composite media, Lecture Notes in Physics No. 272, Springer, Berlin, 1987.

[2] P. Suquet, Continuum micromechanics, CISM Courses and Lectures No. 377, Springer Verlag, Berlin, 1997.

[3] L.P. Kubin, G. Canova, M. Condat, B. Devincre, V. Pontikis, Y. Bréchet, Dislocation microstructures and plastic flow: a 3D simulation, Solid State Phenom. 23&24 (1992) 455–465.

[4] S. Forest, F. Barbe, G. Cailletaud, Cosserat modelling of size effects in the mechanical behaviour of polycrystals and multiphase materials, Int. J. Solids Struct. 37 (2000) 7105–7126.

[5] R. Parisot, S. Forest, A.-F. Gourgues, A. Pineau, D. Mareuse, Modeling the mechanical behavior of a multicrystalline zinc coating on a hot-dip galvanized steel sheet, Comput. Mater. Sci. 19 (2001) 189–204.

[6] F. Eberl, F. Feyel, S. Quilici, G. Cailletaud, Approches numériques de la plasticité cristalline, J. Phys. IV France 8 (1998) Pr4-15–Pr4-25.

[7] F. Eberl, Second order heterogeneities in a multicrystal: experimental developments using X-ray diffraction and comparison with a finite element model, Thèse de doctorat, Doctor Communitatis Europae ENSAM Paris, 2000.

[8] K. Schmidegg, Finite element simulation of local deformations in polycrystals and comparison to experimental results, in: Diplomarbeit, Montanuniversität Leoben, 2000.

[9] J.S. Stölken, Finite element simulation of a 1000 grain virtual test sample, in: J. Bassani, H. Gao, L. Kubin, R.L.P. Selinger (Eds.), Material Research Society Fall Meeting, Symposium Z: Multiscale Materials Modeling, Boston, 27 November–1 December 2000.

[10] L.J. Gibson, M.F. Ashby, Cellular Solids, Cambridge University Press, 1998.

[11] E. Maire, F. Wattebled, J.Y. Buffiere, G. Peix, Deformation of a metallic foam studied by X-ray computed tomography and finite element calculations, in: T.W. Clyne, A.B. Simancik (Eds.), Proceedings of the 'Euromat 99' Conference in München, vol. 5, Wiley vch (Phs), 1999, pp. 68–73.

[12] X. Badiche, S. Forest, T. Guibert, Y. Bienvenu, J.-D. Bartout, P. Ienny, M. Croset, H. Bernet, Mechanical properties and non-homogeneous deformation of open-cell nickel foams: application of the mechanics of cellular solids and of porous materials, Mater. Sci. Eng. A A289 (2000) 276–288.

[13] F. Grillon, communication personnelle, 2001.

[14] Y. El Ouarzazi, Mechanical properties of a highly-contrasted two-phase material, Technical report, Ecole des Mines de Paris, 2000.

[15] M. Bornert, T. Bretheau, P. Gilormini, Homogénéisation en Mécanique des Matériaux, Hermès, 2001.

[16] F. Barbe, L. Decker, D. Jeulin, G. Cailletaud, Intergranular and intragranular behavior of polycrystalline aggregates. Part 1: FE model, Int. J. Plast. 17 (2001) 513–536.

[17] F. Barbe, S. Forest, G. Cailletaud, Intergranular and intragranular behavior of polycrystalline aggregates. Part 2: Results, Int. J. Plast. 17 (2001) 537–563.

[18] J. Besson, G. Cailletaud, J.-L. Chaboche, S. Forest, Mécanique Non Linéaire des Matériaux, Hermès, France, 2001, 445 p.

[19] A.G. Khachaturyan, Theory of Structural Transformations in Solids, John Wiley & Sons, 1983.

[20] Y. Wang, A.G. Khachaturyan, J.W. Morris Jr., A two-dimensional analysis of the evolution of coherent precipitates in elastic media, Acta Metall. Mater. 41 (1993) 325–336.

[21] H. Moulinec, P. Suquet, A fast numerical method for computing the linear and non linear mechanical properties of composites, C.R. Acad. Sci. Paris 318 (1994) 1417–1423.

[22] P.L. George, H. Borouchaki, Triangulation de Delaunay et Maillage. Applications aux élément Finis, Hermès, 1997.

[23] J.F. Thompson, B.K. Soni, N.P. Weatherill, Handbook of Grid Generation, CRC Press, 1999.

[24] S. Ghosh, K. Lee, S. Moorthy, Two-scale analysis of heterogeneous elastic–plastic materials with asymptotic homogenization and Voronoi cell finite element model, Comput. Meth. Appl. Mech. Eng. 132 (1996) 63–116.

[25] Z set package. Available from <www.nwnumerics.com>.

[26] C. Farhat, F.-X. Roux, A method of finite element tearing and interconnecting and its parallel solution algorithm, Int. J. Numer. Methods Eng. 32 (1991) 1205–1227.

[27] F. Feyel, Application du calcul parallèle aux modèles à grand nombre de variables internes, Thèse de doctorat, Ecole des Mines de Paris, 1998.

[28] J. Mandel, Equations constitutives et directeurs dans les milieux plastiques et viscoplastiques, Int. J. Solids Struct. 9 (1973) 725–740.

[29] R.J. Asaro, Crystal plasticity, J. Appl. Mech. 50 (1983) 921–934.

[30] A.M. Cuitiño, M. Ortiz, Computational modelling of single crystals, Modell. Simul. Mater. Sci. Eng. 1 (1993) 225–263.

[31] Y. Estrin, Dislocation density related constitutive modelling, in: Unified Constitutive Laws of Plastic Deformation, Academic Press, 1996, pp. 69–106.

[32] L. Méric, P. Poubanne, G. Cailletaud, Single crystal modeling for structural calculations. Part1: Model presentation, J. Eng. Mater. Technol. 113 (1991) 162–170.

[33] L. Méric, G. Cailletaud, M. Gaspérini, FE calculations of copper bicrystal specimens submitted to tension-compression tests, Acta Metall. Mater. 42 (3) (1993) 921–935.

[34] F. Barbe, R. Parisot, S. Forest, G. Cailletaud, Calibrating a homogenization polycrystal model from large scale computations of polycrystalline aggregates, J. Phys. IV 11 (2001) Pr5-277–Pr5-284.

[35] A. Lasalmonie, J.L. Strudel, Influence of grain size on the mechanical behaviour of some high strength materials, J. Mater. Sci. 21 (1985) 1837–1852.

[36] C. Teodosiu, Elastic Models of Crystal Defects, Springer Verlag, Berlin, 1982.
[37] M.F. Ashby, The deformation of plastically non-homogeneous alloys, in: A. Kelly, R.B. Nicholson (Eds.), Strengthening Methods in Crystals, Applied Science Publishers, London, 1971, pp. 137–192.
[38] N.A. Fleck, J.W. Hutchinson, Strain gradient plasticity, Adv. Appl. Mech. 33 (1997) 295–361.
[39] S. Forest, Cosserat modeling of size effects in polycrystals, in: J.L. Bassani, L.P. Kubin, R.L.P. Selinger, K. Cho (Eds.), Multiscale Materials Modeling-2000, vol. 653, Material Research Society, Boston, 2001, pp. Z8.2.1–Z8.2.12.
[40] S. Forest, P. Boubidi, R. Sievert, Strain localization patterns at a crack tip in generalized single crystal plasticity, Scripta Mater. 44 (2001) 953–958.
[41] O. Diard, S. Leclercq, G. Rousselier, G. Cailletaud, Intergranular stress corrosion cracking modelling for zirconium alloy fuel cladding: environmental effects simulations with mechanical–chemical coupled calculations, in: D. Miannay, P. Costa, D. François, A. Pineau (Eds.), EuroMat2000, Proceedings of the Advances in Mechanical Behaviour, Plasticity and Damage, Elsevier, 2000, pp. 1175–1180.
[42] M. Parise, O. Sicardy, G. Cailletaud, Modelling of the mechanical behavior of the metal-oxide system during Zr alloy oxidation, J. Nucl. Mater. 256 (1998) 35–46.
[43] C. Teodosiu, J. Raphanel, L. Tabourot, Finite element simulation of the large elastoplastic deformation of multicrystals, in: C. Teodosiu, F. Sidoroff (Eds.), Large Plastic Deformations MECAMAT'91, Balkema, Rotterdam, 1993, pp. 153–158.
[44] A. Ziegenbein, H. Neuhäuser, J. Thesing, R. Ritter, H. Wittich, E. Steck, M. Levermann, Local plasticity of Cu–Al polycrystals—measurements and FEM simulation, J. Phys. IV France 8 (1998) Pr8-407–Pr8-412.
[45] F. Delaire, J.L. Raphanel, C. Rey, Plastic heterogeneities of a copper multicrystal deformed in uniaxial tension: experimental study and finite element simulations, Acta Mater. 48 (2000) 1075–1087.
[46] C. Rey, P. Viaris de Lesegno, R. Chiron, Analysis of shear localization in iron single crystals by local strain field and lattice rotation field measurements, in: J. Ziebs, J. Bressers, H. Frenz, D.R. Hayhurst, H. Klingelhöffer, S. Forest (Eds.), Proceedings of the International Symposium on Local Strain and Temperature Measurements in Non-uniform Fields at Elevated Temperatures, Woodhead Publishing Limited, Berlin, 1996, pp. 30–39.
[47] F. Eberl, S. Forest, T. Wroblewski, G. Cailletaud, J.-L. Lebrun, Finite element calculations of the lattice rotation field of a tensile loaded nickel base alloy multicrystal and comparison to topographical X-ray diffraction measurements, Metall. Mater. Trans. 33A (2002) 2825–2833.
[48] T. Kanit, S. Forest, I. Galliet, V. Mounoury, D. Jeulin, Determination of the size of the representative volume element for random composites: statistical and numerical approach, Int. J. Solids Struct., to appear.
[49] C. Huet, Application of variational concepts to size effects in elastic heterogeneous bodies, J. Mech. Phys. Sol. 38 (1990) 813–841.
[50] H. Mughrabi, Introduction to the viewpoint set on: surface effect in cyclic deformation and fatigue, Scripta Metall. Mater. 26 (1992) 1499–1504.
[51] R.N. Pangborn, S. Weissmann, I.R. Kramer, Dislocations distribution and prediction of fatigue damage, Metall. Trans. 12A (1981) 109–120.
[52] J.T. Fourie, The flow stress gradient between the surface and centre of deformed copper single crystals, Philos. Mag. 15 (1967) 735–756.
[53] H. Mughrabi, Investigations of plastically deformed copper single crystals in the stress-applied state, Phys. Status Solidi 39 (1970) 317–327.
[54] P. Pilvin, Une approche simplifiée pour schématiser l'effet de surface sur le comportement mécanique d'un polycristal, J. Phys. IV France 4 (1998) Pr4-33–Pr4-38.
[55] M. Sauzay, P. Gilormini, Surface and cyclic microplasticity, Fatigue Fract. Engng. Mater. Struct. 23 (2000) 573–580.
[56] F. Barbe, Modélisation du comportement mécanique d'agrégats polycristallins, Thèse de doctorat, Ecole des Mines de Paris, 2000.
[57] A.J. Beaudoin, K.K. Mathur, P.R. Dawson, G.C. Johnson, Three-dimensional deformation process simulation with explicit use of polycrystal plasticity models, Int. J. Plast. 9 (1993) 833–860.
[58] A. Staroselski, L. Anand, Inelastic deformation of polycrystalline face centered cubic materials by slip and twinning, J. Mech. Phys. Sol. 46 (4) (1998) 671–696.
[59] D.P. Mika, P.R. Dawson, Effects of grain interaction on deformation in polycrystals, Mater. Sci. Eng. A 257 (1998) 62–76.
[60] T.H. Lin, Analysis of elastic and plastic strains of face centered cubic crystal, J. Mech. Phys. Sol. 5 (1957) 143–149.
[61] E. Kröner, Zur plastischen verformung des vielkristalls, Acta Metall. 9 (1961) 155–161.
[62] M. Berveiller, A. Zaoui, An extension of the self-consistent scheme to plastically flowing polycrystal, J. Mech. Phys. Sol. 26 (1979) 325–344.
[63] R. Hill, Continuum micro-mechanics of elastoplastic polycrystals, J. Mech. Phys. Sol. 13 (1965) 89–101.
[64] G. Cailletaud, P. Pilvin, Utilisation de modèles polycristallins pour le calcul par éléments finis, Rev. Eur. Élém. Finis 3 (4) (1994) 515–541.
[65] P. Pilvin, The contribution of micromechanical approaches to the modelling of inelastic behaviour of polycrystals, in: A. Pineau, G. Cailletaud, T. Lindley (Eds.), Fourth International Conference on Biaxial/multiaxial Fatigue and Design, ESIS 21, Mechanical Engineering Publications, London, 1996, pp. 3–19.
[66] T. Kanit, S. Forest, D. Jeulin, V. Mounoury, I. Galliet, Détermination du volume élémentaire représentatif d'un milieu élastique aléatoire, Technical report, GT Mécamat

Approches probabilistes en mécanique des milieux hétérogènes, organisé par D. Jeulin, F. Montheillet, P. Franciosi, INSA-Lyon, 31 mai 2001.

[67] S. Quilici, S. Forest, G. Cailletaud, On size effects in torsion of multi- and polycrystalline specimens, J. Phys. IV 8 (1998) Pr8-325–Pr8-332.